Clinical Contributors to Cerebral White Matter Integrity in HIV-infected Individuals

Assawin Gongvatana, PhD[a], Ronald A. Cohen, PhD[a], Stephen Correia, PhD[a], Kathryn N. Devlin, BS[a], Jadrian Miles, ScM[b], Hakmook Kang, MS[c], Hernando Ombao, PhD[c], Bradford Navia, MD, PhD[d], David H. Laidlaw, PhD[b], Karen T. Tashima, MD[a]

[a]Warren Alpert Medical School of Brown University, [b]Brown University Department of Computer Science, [c]Brown University Department of Biostatistics, [d]Tufts University School of Medicine

Supported by NIH R01MH07436803 and P30AI042853 (Lifespan/Tufts/Brown Center for AIDS Research)

Address correspondence to:
Ronald A. Cohen, Ph.D.
1 Hoppin St
Providence, RI 02908
(401) 793-8787
rcohen@lifespan.org

INTRODUCTION

HIV-infected individuals frequently exhibit brain dysfunction, typically involving activated microglia, infiltrating peripheral macrophages, and astrocytosis[1]. Myelin pallor, synaptodendritic injury, and axonal damage have been reported in post mortem brains of individuals with advanced disease[2-5]. Structural MRI studies have showed preferential damage to cerebral white matter and subcortical brain structures[6,7]. While severe disturbances in neurocognitive and everyday functions have become relatively rare in HIV-infected (HIV+) people since the advent of combination antiretroviral therapy (CART), recent data have demonstrated the persistence of milder forms of HIV-associated neurocognitive disorder, with a reported estimate close to 50% in a national US cohort[8].

Given such high prevalence of abnormalities even in medically stable people with largely reconstituted immune function and suppressed viral loads, the etiology of HIV-associated brain dysfunction in the CART era remains unclear. Recent studies utilizing structural and metabolic neuroimaging markers have found nadir CD4 levels to be related to brain abnormalities in medically stable HIV+ individuals[9,10], indicating the importance of distant history of immune suppression on current brain integrity. Additional possibilities include the various comorbid conditions commonly found in HIV+ people, which may in fact account for a significant part of the observed brain dysfunction. Hepatitis C virus (HCV) is among the most common coinfections with HIV, likely due to shared primary modes of transmission via intravenous drug use and sexual contact. An estimated 30-35% HIV/HCV coinfection rate in the US has been reported[11], and coinfected individuals have been found to exhibit more severe neurocognitive symptoms than those with monoinfection[12].

A number of neuroimaging markers have been utilized to examine the etiology of brain dysfunction in people with chronic HIV infection. Considering the multifaceted nature of the neuropathology, it is important that the measured brain changes be considered in the context of the multiple clinical contributors, including factors directly related to the HIV disease (i.e., CD4 level, HIV viral load, duration of infection, CART status), as well as other relevant factors with significant CNS effects, including HCV coinfection and aging. The independent contributions and relative importance of these factors on measures of brain abnormalities can then be examined. To date, such comprehensive analysis is still lacking in the literature.

Diffusion tensor imaging (DTI) is an analytical approach for diffusion weighted MRI data that allows the quantification of microstructural water diffusion characteristics[13]. DTI studies in HIV have found significant abnormalities in measures of anisotropy and diffusivity, indicating

microstructural damage in various cerebral white matter regions, particularly in regions of interest (ROI) placed in the white matter of the frontal lobes and the corpus callosum[14-19]. Subsequent studies utilizing voxelwise analysis rather than a priori ROIs, however, have found more widespread HIV-associated white matter damage that are not limited to previously identified regions[20-22]. Such findings are consistent with the diffuse neuropathology of HIV infection[1], and underline the importance of a comprehensive examination of brain regions and their relationships to the multiple potential clinical contributors. Recent developments in methods for anatomical parcellation of high-resolution MRI images have enabled accurate and detailed definition of cerebral white matter regions throughout the brain[23-25]. When acquired concurrently with diffusion MRI images, such white matter parcellations can be used to query white matter integrity in regions encompassing all lobes of the brain, and thus provide an alternative approach to voxelwise analysis, which can be methodologically challenging to implement in DTI[26].

The current study utilized a multivariable statistical approach to examine the effects of important clinical variables on the microstructural integrity in white matter regions defined throughout the brain. Specifically, we examined the independent effects of HIV disease markers, CART status, age, and HCV coinfection on DTI measures in each brain region. We hypothesized that worse immune function, higher viral load, longer infection duration, lack of treatment, older age, and HCV coinfection would be associated with worse cerebral white matter integrity in the brain regions examined.

METHODS

Participants

Participants include 85 HIV-infected (HIV+) individuals aged 23 to 65 who were recruited as part of an NIH-sponsored study of HIV-associated brain dysfunction at The Miriam Hospital / Brown University. The study was approved by the institutional review board, and informed consent was obtained from each participant prior to enrollment. Exclusion criteria included 1) history of head injury with loss of consciousness > 10 minutes; 2) neurological conditions including dementia unrelated to HIV, seizure disorder, stroke, and opportunistic infection of the brain; 3) severe psychiatric illness that may impact brain function, e.g., schizophrenia; and 4) substance use disorder within 6 months prior to neuroimaging.

HIV serostatus was documented by ELISA and confirmed by Western blot test. Most participants (81%) were treated with combination antiretroviral therapy (CART), and generally

had well-controlled HIV viral load and intact immune function: 68% had undetectable plasma HIV RNA (<75 copies/ml), average CD4 count was 438. More than half (58%) of the participants reported nadir CD4 < 200, indicating history of significant immune suppression. A significant number (33%) of participants had current hepatitis C infection (HCV+), defined as detectable serum HCV RNA by PCR. Table 1 shows relevant demographic and clinical information of participants.

MRI Data Acquisition

All neuroimaging was performed on one Siemens Tim Trio 3-tesla MRI imager located at Brown University MRI Research Facility. Diffusion weighted MRI was acquired using a double-spin-echo echo-planar pulse sequence in the axial plane with TE = 103ms, TR = 10060ms, in-plane resolution = 1.77mm x 1.77mm, slice thickness = 1.8mm prescribed to cover the whole brain. Diffusion-weighted images (DWI) with b-value = 1000 s/mm^2 were acquired in 64 diffusion gradient directions. Ten images with no diffusion encoding (non-DWI) were acquired as baseline for diffusion tensor fitting. Due to scanner operating system upgrade during the study, an identical protocol with the exception of TR = 10100ms was used for 20 participants. This protocol difference was accounted for during statistical analysis. High-resolution structural MRI of the whole brain was acquired in the sagittal plane using a T1-weighted MPRAGE pulse sequence with TE/TR = 3.06/2250ms, flip angle = 9°, resolution = 0.86mm x 0.86mm x 0.86mm.

Diffusion Tensor Analysis

All image registrations were performed using FSL FLIRT[27] with mutual information cost function. The non-DWI images were co-registered using 6-parameter rigid body registrations to correct for movement. To increase signal-to-noise ratio, these co-registered images were averaged and used as baseline for subsequent tensor fitting. The 64 DWIs were registered to this average non-DWI image using 12-parameter affine registrations to account for movement and eddy current-induced distortions. To account for the spatial transformations, the diffusion gradient vectors for individual DWIs were adjusted according to the corresponding affine transformations[28]. Diffusion tensor estimations were performed using a nonlinear iterative method in order to avoid negative eigenvalues[29]. The three principal eigenvectors and associated eigenvalues of the tensor characterizing the diffusion ellipsoid were then computed. Fractional anisotropy (FA) and mean diffusivity (MD) were derived from the eigenvalues using standard formulas[13].

Segmentation of White Matter Regions of Interest

Segmentation of brain tissues and identification of cortical landmarks were performed on each T1-weighted MRI image using an automated set of algorithms implemented in Freesurfer[23]. White matter voxels underlying the cortex were subsequently segmented and labeled based on the spatial proximity of each voxel to the identified cortical landmarks. The segmentation algorithm and anatomical locations of the regions were previously described in detail[24,25]. Using this approach, we derived 29 white matter regions of interest (ROI) in each hemisphere, consisting of 10 regions in the frontal lobe, 10 regions in the temporal lobe, five regions in the parietal lobe, and four regions in the occipital lobe (Figure 1). Bilateral ROIs were combined for the purpose of the current analysis. This strategy was implemented both to minimize the number of multiple comparisons and increase the number of voxels comprising each ROI.

Rigid-body registrations between the T1 and average non-DWI images were then performed using FLIRT with mutual information to account for head movements. The resulting transformations were applied to the segmented ROIs, using nearest-neighbor interpolation to preserve the integer labels. To account for partial voluming and to ensure inclusion of only white matter voxels, transformed ROIs were further refined by applying an FA threshold of 0.3. Average FA and MD values in each ROI were computed as measures of white matter integrity in the corresponding region for use in the subsequently statistical analysis.

Statistical Analysis

All statistical analysis was performed in R version 2.12.1[30]. For each ROI, a multivariable regression model was fitted to simultaneously examine the white matter effects of age, HCV coinfection, current CD4 level, nadir CD4, plasma HIV RNA, HIV infection duration, and current CART regimen. Age, current CD4, infection duration were included as continuous variables. Categorical coding was used for HCV coinfection (non-infected/infected) and HIV RNA (undetectable/detectable). Nadir CD4 was categorized into two groups using a cutoff of 200 (AIDS-defining) due to a skewed distribution. Additionally, diffusion imaging protocol was included as a covariate (see description of data acquisition). Specifically, the following regression model was used, testing the null hypothesis $\beta_i=0$: $Y = \beta_0 + \beta_1*(\text{age}) + \beta_2*(\text{HCV}) + \beta_3*(\text{CD4}) + \beta_4*(\text{CD4 nadir}) + \beta_5*(\text{HIV RNA}) + \beta_6*(\text{infection duration}) + \beta_7*(\text{CART}) + \beta_8*(\text{diffusion protocol}) + \varepsilon$, where Y reflects FA or MD in each ROI. The statistical test for each regression coefficient thus reflects the unique effect of each clinical variable on white matter integrity after controlling for all the other variables. False discovery rate (FDR) was used to control for multiple

comparisons for ROIs within each lobe of the brain. The FDR approach controls for the expected proportion of falsely rejected hypotheses, and has been shown to yield higher statistical power than traditional corrections for familywise error rate while controlling for type I error level. An FDR threshold of $q \leq .1$ was used to define statistical significance in all analyses[31].

RESULTS

Figure 2 and Table 2 show the regression coefficients and associated p-values for clinical variables with significant effects (FDR $q \leq .1$) on fractional anisotropy (FA) and mean diffusivity (MD) in the white matter ROIs. Figure 2 shows regions with significant effects of clinical variables on white matter abnormalities. Unless otherwise noted, the directions of the effects of the clinical variables are as hypothesized, with decreased FA and increased MD indicating white matter damage.

Frontal Lobes

Significant effects of HCV coinfection and age were found on frontal white matter integrity. HCV coinfection was associated with decreased FA in regions underlying the rostral middle frontal gyrus ($p = .016$) and medial orbitofrontal cortex ($p = .0189$). Older age was associated with decreased FA in all frontal white matter regions examined, including regions underlying the superior frontal gyrus ($p = .0004$), rostral middle frontal gyrus ($p = .0023$), caudal middle frontal gyrus ($p = .0024$), pars opercularis ($p = .0158$), pars triangularis ($p = .0189$), pars orbitalis ($p = .0179$), lateral orbitofrontal cortex ($p = .0002$), medial orbitofrontal cortex ($p = .0001$), precentral gyrus ($p = .0769$), and paracentral lobule ($p = .0019$). No significant effects on MD in the frontal ROIs were found.

Temporal Lobes

Significant effects of HCV, current antiretroviral treatment, and age were found on measures of white matter integrity in the temporal lobes. Significant effects of HCV coinfection on FA and MD were found in the majority of temporal regions: HCV was associated with decreased FA in regions underlying the fusiform gyrus ($p = .0285$), inferior temporal gyrus ($p = .0246$), and banks of the superior temporal sulcus ($p = .0267$); and increased MD in regions underlying the entorhinal cortex ($p = .018$), parahippocampal gyrus ($p = .0361$), fusiform gyrus ($p = .0332$), inferior temporal gyrus ($p = .021$), and banks of the superior temporal sulcus ($p =$

.0216). Current CART treatment was associated with better white matter integrity in the temporal lobes, as indicated by increased FA in regions underlying the parahippocampal gyrus ($p = .0178$), fusiform gyrus ($p = .0195$), and banks of the superior temporal sulcus ($p = .0301$). Older age was associated with decreased FA in regions underlying the fusiform gyrus ($p = .0158$), inferior temporal gyrus ($p = .0386$), banks of the superior temporal sulcus ($p = .0141$), and insular cortex ($p = .0072$).

Parietal Lobes

Significant effects of HCV, current CD4 level, and age were found on parietal white matter integrity. HCV coinfection was associated with increased MD in regions underlying the inferior parietal cortex ($p = .0382$) and precuneus cortex ($p = .0117$). Higher current CD4 level was associated with better white matter integrity as indicated by increased FA in regions underlying the superior parietal cortex ($p = .0415$) and inferior parietal cortex ($p = .0268$). Older age was associated with decreased FA in regions underlying the supramarginal gyrus ($p = .054$), superior parietal cortex ($p = .0366$), and inferior parietal cortex ($p = .0004$).

Occipital Lobes

HCV coinfection was associated with increased MD in white matter regions in the occipital lobes, including in regions underlying the lingual gyrus ($p = .0249$), cuneus cortex ($p = .0623$), and lateral occipital cortex ($p = .0273$). Contrary to expectation, older age was associated with decreased MD in region underlying the cuneus cortex ($p = .0041$). No significant effects on FA in the occipital ROIs were found.

DISCUSSION

Abnormal changes in white matter integrity were found to be associated with a number of clinical variables in this cohort of medically stable HIV-infected individuals. These findings provide insights into the brain dysfunction in people living with HIV in the era of combination antiretroviral therapy (CART), since most participants were CART-treated and exhibited largely reconstituted immune function at the time of the study. DTI indices of white matter integrity were derived from 29 cerebral white matter regions, which were segmented on each individual brain using a high-resolution T1-weighted image. Significant effects of clinical variables, including HCV coinfection, age, current CD4 level, and CART status, were found on white matter abnormalities in virtually all brain regions examined. Most notably, HCV coinfection and older

age were associated with white matter injury, reflected by decreased anisotropy or increased diffusivity, in the majority of brain regions examined. In addition, individuals with higher current CD4 level exhibited higher anisotropy in parietal lobe regions, while those undergoing CART regimens exhibited higher anisotropy in temporal lobe regions (see Figure 2). To our knowledge, this is the first study to specifically examine the individual contributions of such clinical markers using a multivariate approach on white matter integrity in regions spanning all lobes of the brain.

The observed pervasive effects of HCV coinfection are particularly noteworthy, especially considering the growing evidence indicating direct involvement of HCV in the CNS[32-34]. A number of neuroimaging studies have reported effects of HCV on the brain, including abnormal cerebral metabolite levels in both grey and white matter regions and abnormalities in whole-brain DTI measures[21,35-37]. Possible synergistic effects of HIV and HCV infections on brain dysfunction have also been reported[12]. We found the majority of HCV-associated white matter changes in the temporal lobes, including areas adjacent to medial temporal structures. Interestingly, this is consistent with recent evidence showing increasing involvement of these cortical structures in HIV-infected people in the CART era[9,38,39]. These findings thus underline the importance of comorbid conditions such as HCV when examining HIV-associated brain dysfunction. Although none of the study participants had a 6-month history of substance use disorder, a substantial proportion (86%) of HCV+ participants reported a lifetime history of cocaine or opiate use. Thus, the residual confounding effects of distant substance use cannot be ruled out as possible explanation for the observed HCV effects. HCV effects were found on measures of both anisotropy and diffusivity. The microstructural changes underlying abnormalities in each of these measures still remain unclear. This pattern of white matter changes may reflect regionally specific HCV neuropathological processes. It is also possible that distinct preexisting microstructural environments are differentially affected by a common disease process, and these possibilities should be investigated in future studies.

Current CD4 count was found to be related to better white matter integrity in the parietal lobes, while CART appears to have positive impact on white matter in the temporal lobes. (It should be noted that the observed effects of CART were not in the direction of drug toxicity as has been reported in some recent studies [REF].) No significant effects of nadir CD4, plasma HIV viral load, or duration of HIV infection were found. It is possible that these results may reflect the selective vulnerability of these specific brain regions to immune suppression or lack of antiretroviral treatment. However, it is also possible that the limited effects of HIV disease markers observed here may reflect the homogeneity in HIV disease characteristics in this

CART-treated, medically stable, cohort of HIV-infected individuals, such as typically found in many relatively resource-rich settings such as the US.

Not surprisingly, older age was among the strongest predictors of white matter injury. These effects were most prominent in the frontal lobes, where decreased anisotropy related to older age was found in all regions. Although these findings are consistent with the substantial body of evidence on age-related white matter damage[40], it is possible that the robust associations observed here may reflect the augmented effects of aging such as has been suggested in the context of HIV infection[41,42]. To further address this point, we conducted exploratory follow-up analyses in this cohort to examine the statistical interactions between age and HIV disease markers. Although no significant interactions were found, the possibility of accelerated brain aging remains an important topic that should be explored in future studies that are adequately powered to perform analyses with additional explanatory variables.

The current findings underline the multifactorial nature of HIV-associated brain dysfunction in the CART era, and the importance of examining the effect of HIV disease in the context of other comorbidities, in particular HCV coinfection and aging. The observed diffuse pattern of white matter injury related to clinical variables is consistent with the diffuse pattern of HIV-associated brain injury. Future neuroimaging studies should therefore employ methodologies that are not limited to circumscribed regions of interest.

Despite recent evidence indicating nadir CD4 as an important predictor of current brain function, we did not find significant effects of this variable on any of the white matter regions examined. Additional possible explanations for the persistence of brain dysfunction include the effects of latent infection as reflected by HIV DNA[43], and limited CNS penetration of antiretroviral drugs[44]. Future studies should examine the contribution of these variables on measures of brain integrity.

The current study utilized a cross sectional study design, which has some inherent limitations. Future longitudinal studies would allow both a better control of potential confounding variables, and the examination of the trajectory of white matter alterations in the context of clinical variables. Finally, future studies utilizing advanced neuroimaging methodologies including diffusion MRI tractography and functional MRI, in combination with neurocognitive measures, will help to further elucidate the effects of HIV and HCV infections on the brain.

REFERENCES

1. Anthony IC, Bell JE. The Neuropathology of HIV/AIDS. *Int Rev Psychiatry*. 2008;20(1):15-24.

2. Gray F, Lescs MC. HIV-related demyelinating disease. *Eur J Med*. 1993;2(2):89-96.

3. Masliah E, Heaton RK, Marcotte TD, et al. Dendritic injury is a pathological substrate for human immunodeficiency virus-related cognitive disorders. HNRC Group. The HIV Neurobehavioral Research Center. *Annals of neurology*. 1997;42(6):963-972.

4. Everall IP, Heaton RK, Marcotte TD, et al. Cortical synaptic density is reduced in mild to moderate human immunodeficiency virus neurocognitive disorder. HNRC Group. HIV Neurobehavioral Research Center. *Brain Pathol.* 1999;9(2):209-217.

5. Giometto B, An SF, Groves M, et al. Accumulation of beta-amyloid precursor protein in HIV encephalitis: relationship with neuropsychological abnormalities. *Annals of neurology*. 1997;42(1):34-40.

6. Stout JC, Ellis RJ, Jernigan TL, et al. Progressive cerebral volume loss in human immunodeficiency virus infection: a longitudinal volumetric magnetic resonance imaging study. HIV Neurobehavioral Research Center Group. *Archives of neurology*. 1998;55(2):161-168.

7. Jernigan TL, Archibald S, Hesselink JR, et al. Magnetic resonance imaging morphometric analysis of cerebral volume loss in human immunodeficiency virus infection. The HNRC Group. *Archives of neurology*. 1993;50(3):250-255.

8. Heaton RK, Clifford DB, Franklin DR, et al. HIV-associated neurocognitive disorders persist in the era of potent antiretroviral therapy: CHARTER Study. *Neurology*. 2010;75(23):2087-2096.

9. Cohen RA, Harezlak J, Schifitto G, et al. Effects of nadir CD4 count and duration of human immunodeficiency virus infection on brain volumes in the highly active antiretroviral therapy era. *J. Neurovirol.* 2010;16(1):25-32.

10. Cohen RA, Harezlak J, Gongvatana A, et al. Cerebral metabolite abnormalities in human immunodeficiency virus are associated with cortical and subcortical volumes. *J. Neurovirol.* 2010.

11. Verucchi G, Calza L, Manfredi R, Chiodo F. Human immunodeficiency virus and hepatitis C virus coinfection: epidemiology, natural history, therapeutic options and clinical management. *Infection*. 2004;32(1):33-46.

12. Hinkin CH, Castellon SA, Levine AJ, Barclay TR, Singer EJ. Neurocognition in individuals co-infected with HIV and hepatitis C. *J Addict Dis*. 2008;27(2):11-17.

13. Basser PJ, Jones DK. Diffusion-tensor MRI: theory, experimental design and data analysis - a technical review. *NMR Biomed*. 2002;15(7-8):456-467.

14. Filippi CG, Ulug AM, Ryan E, Ferrando SJ, van Gorp W. Diffusion tensor imaging of patients with HIV and normal-appearing white matter on MR images of the brain. *AJNR Am J Neuroradiol*. 2001;22(2):277-283.

15. Pfefferbaum A, Rosenbloom MJ, Rohlfing T, et al. Frontostriatal fiber bundle compromise in HIV infection without dementia. *AIDS*. 2009;23(15):1977-1985.

16. Pomara N, Crandall DT, Choi SJ, Johnson G, Lim KO. White matter abnormalities in HIV-1 infection: a diffusion tensor imaging study. *Psychiatry Res*. 2001;106(1):15-24.

17. Ragin AB, Wu Y, Storey P, et al. Diffusion tensor imaging of subcortical brain injury in patients infected with human immunodeficiency virus. *J. Neurovirol.* 2005;11(3):292-298.

18. Wu Y, Storey P, Cohen BA, et al. Diffusion alterations in corpus callosum of patients with HIV. *AJNR Am J Neuroradiol*. 2006;27(3):656-660.

19. Thurnher MM, Castillo M, Stadler A, et al. Diffusion-tensor MR imaging of the brain in human immunodeficiency virus-positive patients. *AJNR Am J Neuroradiol*. 2005;26(9):2275-2281.

20. Chen Y, An H, Zhu H, et al. White matter abnormalities revealed by diffusion tensor imaging in non-demented and demented HIV+ patients. *Neuroimage*. 2009;47(4):1154-1162.

21. Stebbins GT, Smith CA, Bartt RE, et al. HIV-associated alterations in normal-appearing white matter: a voxel-wise diffusion tensor imaging study. *J Acquir Immune Defic Syndr*. 2007;46(5):564-573.

22. Gongvatana A, Schweinsburg BC, Taylor MJ, et al. White matter tract injury and cognitive impairment in human immunodeficiency virus-infected individuals. *J. Neurovirol.* 2009;15(2):187-195.

23. Fischl B, Salat DH, van der Kouwe AJ, et al. Sequence-independent segmentation of magnetic resonance images. *Neuroimage*. 2004;23 Suppl 1:S69-84.

24. Desikan RS, Ségonne F, Fischl B, et al. An automated labeling system for subdividing the human cerebral cortex on MRI scans into gyral based regions of interest. *Neuroimage*. 2006;31(3):968-980.

25. Salat DH, Greve DN, Pacheco JL, et al. Regional white matter volume differences in nondemented aging and Alzheimer's disease. *Neuroimage*. 2009;44(4):1247-1258.

26. Smith SM, Jenkinson M, Johansen-Berg H, et al. Tract-based spatial statistics: voxelwise analysis of multi-subject diffusion data. *Neuroimage*. 2006;31(4):1487-1505.

27. Smith SM, Jenkinson M, Woolrich MW, et al. Advances in functional and structural MR image analysis and implementation as FSL. *Neuroimage*. 2004;23 Suppl 1:S208-19.

28. Alexander DC, Pierpaoli C, Basser PJ, Gee JC. Spatial transformations of diffusion tensor magnetic resonance images. *IEEE Trans Med Imaging*. 2001;20(11):1131-1139.

29. Cox RW. AFNI: software for analysis and visualization of functional magnetic resonance neuroimages. *Comput Biomed Res*. 1996;29(3):162-173.

30. *R Development Core Team. R: A Language and Environment for Statistical Computing. *Vienna Austria R Foundation for Statistical Computing*. 2010;1(09/18/2009).

31. Benjamini Y, Hochberg Y. Controlling the False Discovery Rate - a Practical and Powerful Approach to Multiple Testing. *J Roy Stat Soc B Met*. 1995;57(1):289-300.

32. Maggi F, Giorgi M, Fornai C, et al. Detection and quasispecies analysis of hepatitis C virus in the cerebrospinal fluid of infected patients. *J. Neurovirol.* 1999;5(3):319-323.

33. Laskus T, Radkowski M, Bednarska A, et al. Detection and analysis of hepatitis C virus sequences in cerebrospinal fluid. *J. Virol.* 2002;76(19):10064-10068.

34. Letendre S, Paulino AD, Rockenstein E, et al. Pathogenesis of hepatitis C virus coinfection in the brains of patients infected with HIV. *J Infect Dis*. 2007;196(3):361-370.

35. Forton DM, Hamilton G, Allsop JM, et al. Cerebral immune activation in chronic hepatitis C infection: a magnetic resonance spectroscopy study. *J Hepatol*. 2008;49(3):316-322.

36. McAndrews MP, Farcnik K, Carlen P, et al. Prevalence and significance of neurocognitive dysfunction in hepatitis C in the absence of correlated risk factors. *Hepatology*. 2005;41(4):801-808.

37. Weissenborn K, Krause J, Bokemeyer M, et al. Hepatitis C virus infection affects the brain-evidence from psychometric studies and magnetic resonance spectroscopy. *J Hepatol*. 2004;41(5):845-851.

38. Cysique LA, Maruff P, Brew BJ. Prevalence and pattern of neuropsychological impairment in human immunodeficiency virus-infected/acquired immunodeficiency syndrome (HIV/AIDS) patients across pre- and post-highly active antiretroviral therapy eras: a combined study of two cohorts. *J. Neurovirol.* 2004;10(6):350-357.

39. Brew BJ. Evidence for a change in AIDS dementia complex in the era of highly active antiretroviral therapy and the possibility of new forms of AIDS dementia complex. *AIDS*. 2004;18 Suppl 1:S75-8.

40. Sullivan EV, Pfefferbaum A. Diffusion tensor imaging and aging. *Neurosci Biobehav Rev*. 2006;30(6):749-761.

41. Valcour V, Shikuma C, Shiramizu B, et al. Higher frequency of dementia in older HIV-1 individuals: the Hawaii Aging with HIV-1 Cohort. *Neurology*. 2004;63(5):822-827.

42. Kirk JB, Goetz MB. Human immunodeficiency virus in an aging population, a complication of success. *J Am Geriatr Soc*. 2009;57(11):2129-2138.

43. Shiramizu B, Williams AE, Shikuma C, Valcour V. Amount of HIV DNA in peripheral blood mononuclear cells is proportional to the severity of HIV-1-associated neurocognitive disorders. *J Neuropsychiatry Clin Neurosci*. 2009;21(1):68-74.

44. Letendre S, Marquie-Beck J, Capparelli E, et al. Validation of the CNS Penetration-Effectiveness rank for quantifying antiretroviral penetration into the central nervous system. *Archives of neurology*. 2008;65(1):65-70.

Figure 1. White matter regions of interest segmented from high resolution T1 image and registered to diffusion image space. Regions are displayed against a background of axial fractional anisotropy (FA) slices. The segmentation algorithm and anatomical locations of the regions were previously described[24,25]. The slice numbers (Z) relative to the most inferior acquired slice are indicated on each image.

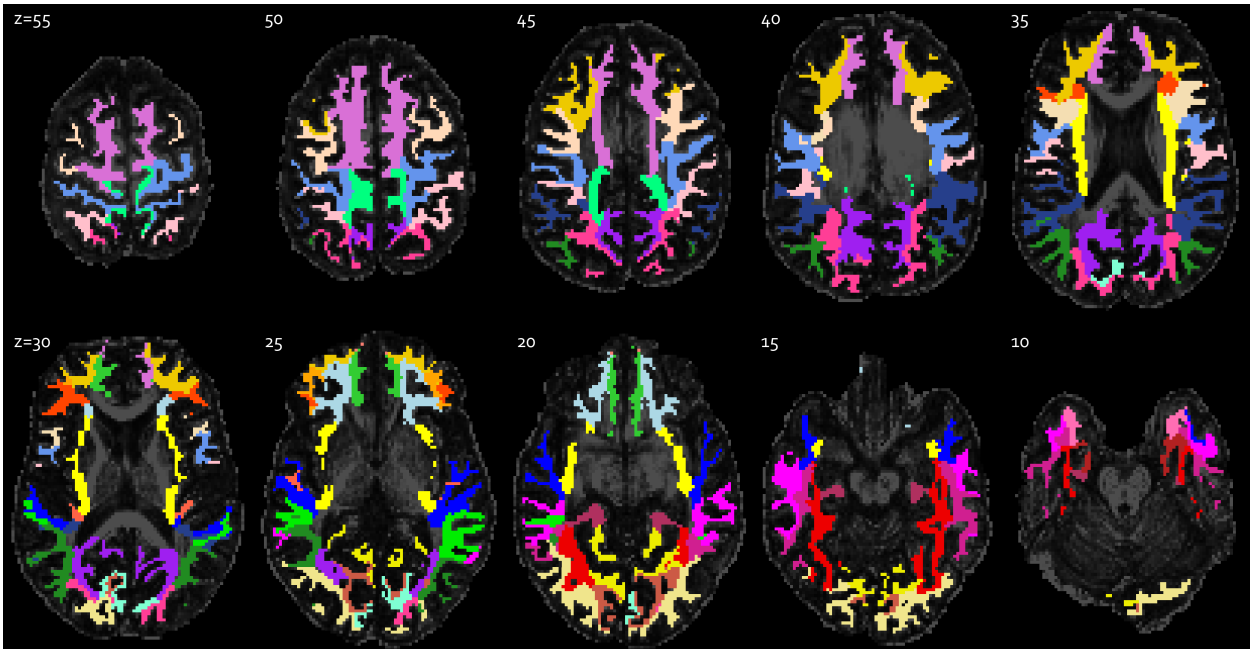

Figure 2. Regression coefficients with 95% confidence interval indicating the effects of clinical variables on fractional anisotropy (FA) and mean diffusivity (MD) in white matter regions underlying 29 cortical landmarks encompassing four lobes of the brain. Variables showing significant (FDR q≤.1) are highlighted along with associated p-values. White matter damage is indicated by decreased FA and increased MD.

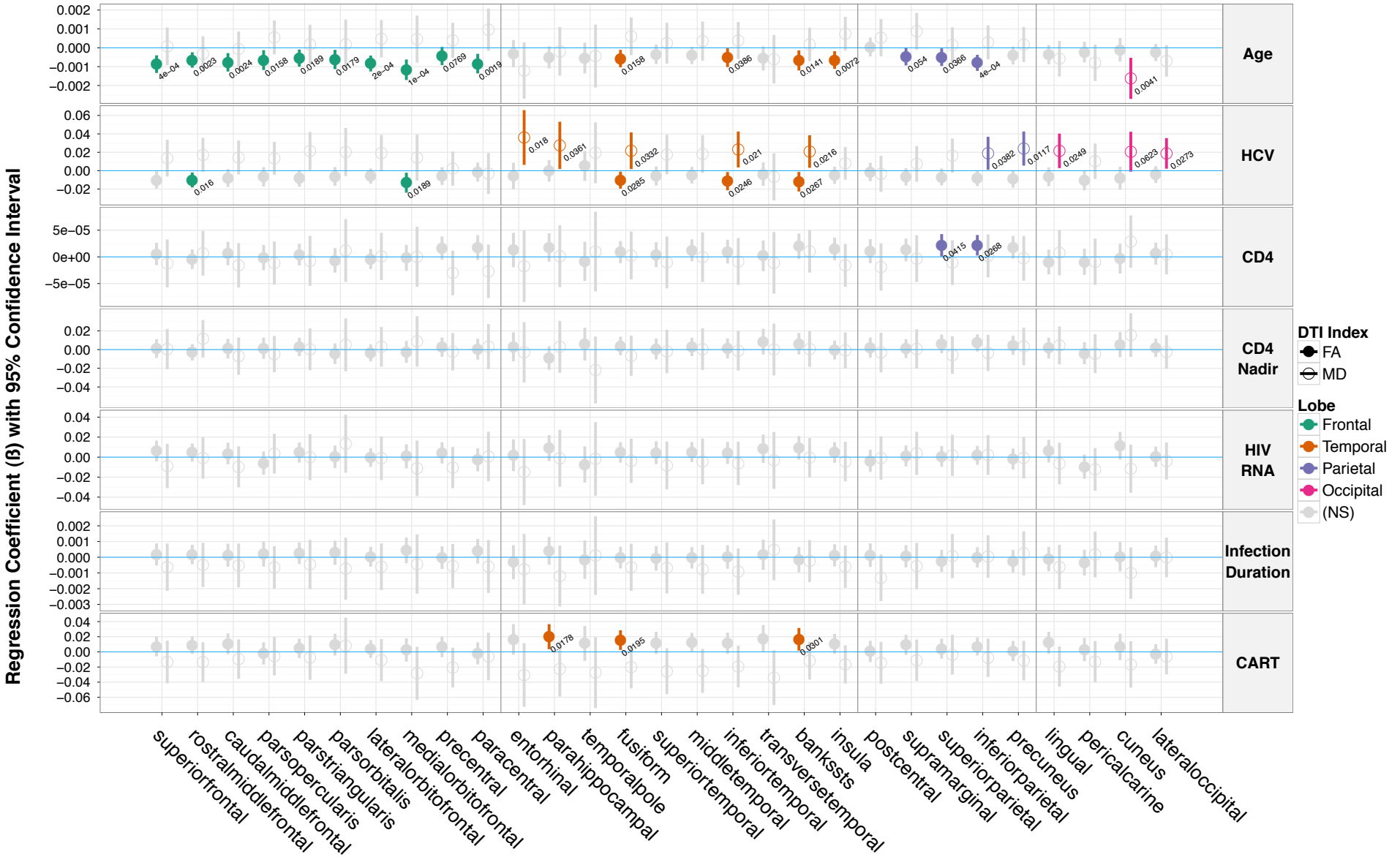

Note: superiorfrontal = superior frontal gyrus, rostralmiddlefrontal = rostral middle frontal gyrus, caudalmiddlefrontal = caudal middle frontal gyrus, parsopercularis = pars opercularis, parstriangularis = pars triangularis, parsorbitalis = pars orbitalis, lateralorbitofrontal = lateral orbitofrontal cortex, medialorbitofrontal = medial orbitofrontal cortex, precentral = precentral gyrus, paracentral = paracentral lobule, entorhinal = entorhinal cortex, parahippocampal = parahippocampal gyrus, temporalpole = temporal pole, fusiform = fusiform gyrus, superiortemporal = superior temporal gyrus, middletemporal = middle temporal gyrus, inferiortemporal = inferior temporal gyrus, transversetemporal = transverse temporal cortex, bankssts = banks of the superior temporal sulcus, insula = insular cortex, postcentral = postcentral gyrus, supramarginal = supramarginal gyrus, superiorparietal = superior parietal cortex, inferiorparietal = inferior parietal cortex, precuneus = precuneus cortex, lingual = lingual gyrus, pericalcarine = pericalcarine cortex, cuneus = cuneus cortex, lateraloccipital = lateral occipital cortex.

Figure 2. Representative axial slices showing brain regions with significant effects of clinical variables on DTI indices. Green overlay indicates decreased FA, blue indicates increased MD, and red indicates abnormalities in both indices associated with older age, hepatitis C coinfection (HCV), lower current CD4 level, and lack of combination antiretroviral treatment (CART). The slice numbers (Z) relative to the most inferior acquired slice are indicated on each image.

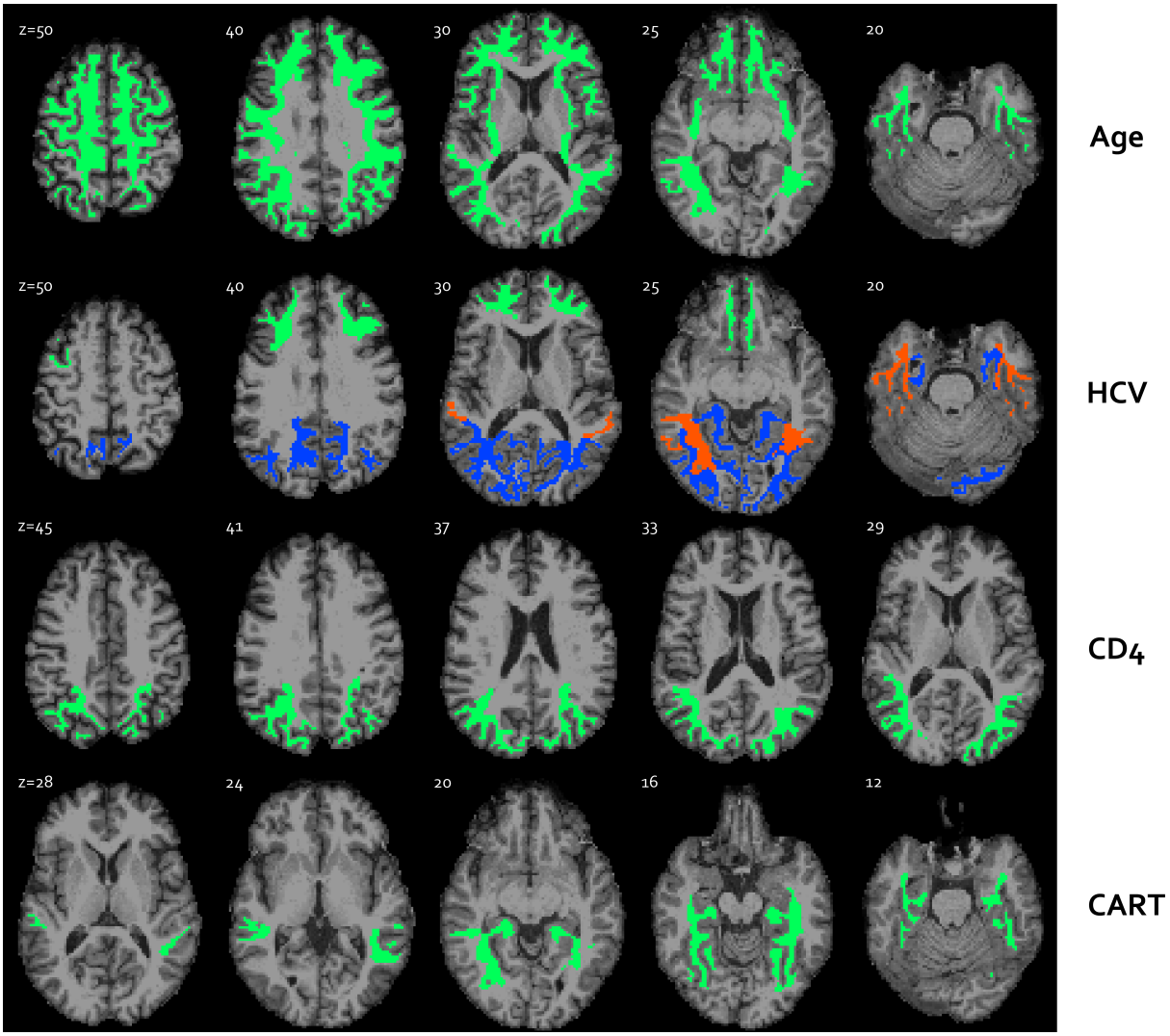

Table 1. Relevant demographic and clinical information of study participants.

N	85
Age (years)	45 ± 9.98
Gender (% male)	57 (67%)
Ethnicity (% Caucasian)	47 (55%)
Current CD4 (cells/ml)	437 ± 221
Nadir CD4 (cells/ml)	184 ± 162
Plasma HIV RNA (% undetectable)	58 (68%)
HIV infection duration (years)	12 ± 7.01
CART-treated (%)	69 (81%)
Current hepatitis C infection (%)	28 (33%)

Note: HCV = hepatitis C virus, CART = combination antiretroviral treatment. Continuous variables are reported as mean±SD. Proportions are reported as N(%).

Table 2. Regression coefficients and associated p-values for clinical variables with significant effects (FDR q ≤ .1) on fractional anisotropy (FA) and mean diffusivity (MD).

DTI Index	Lobe	Clinical Variable	Region	Coefficient	p-value
FA	Frontal	Age	Superior Frontal Gyrus	-0.0009	0.0004
			Rostral Middle Frontal Gyrus	-0.0006	0.0023
			Caudal Middle Frontal Gyrus	-0.0008	0.0024
			Pars Opercularis	-0.0007	0.0158
			Pars Triangularis	-0.0005	0.0189
			Pars Orbitalis	-0.0006	0.0179
			Lateral Orbitofrontal Cortex	-0.0008	0.0002
			Medial Orbitofrontal Cortex	-0.0012	0.0001
			Precentral Gyrus	-0.0004	0.0769
			Paracentral Lobule	-0.0008	0.0019
		HCV	Rostral Middle Frontal Gyrus	-0.0101	0.0160
			Medial Orbitofrontal Cortex	-0.0130	0.0189
	Temporal	Age	Fusiform Gyrus	-0.0006	0.0158
			Inferior Temporal Gyrus	-0.0005	0.0386
			Banks of the Superior Temporal Sulcus	-0.0007	0.0141
			Insular Cortex	-0.0006	0.0072
		HCV	Fusiform Gyrus	-0.0103	0.0285
			Inferior Temporal Gyrus	-0.0114	0.0246
			Banks of the Superior Temporal Sulcus	-0.0120	0.0267
		CART	Parahippocampal Gyrus	0.0201	0.0178
			Fusiform Gyrus	0.0155	0.0195
			Banks Of The Superior Temporal Sulcus	0.0166	0.0301
	Parietal	Age	Supramarginal Gyrus	-0.0005	0.0540
			Superior Parietal Cortex	-0.0005	0.0366
			Inferior Parietal Cortex	-0.0008	0.0004
		CD4	Superior Parietal Cortex	0.00002	0.0415
			Inferior Parietal Cortex	0.00002	0.0268
MD	Temporal	HCV	Entorhinal Cortex	0.0361	0.0180
			Parahippocampal Gyrus	0.0275	0.0361
			Fusiform Gyrus	0.0217	0.0332
			Inferior Temporal Gyrus	0.0231	0.0210
			Banks of the Superior Temporal Sulcus	0.0208	0.0216
	Parietal	HCV	Inferior Parietal Cortex	0.0189	0.0382
			Precuneus Cortex	0.0240	0.0117
	Occipital	Age	Cuneus Cortex	-0.0016	0.0041
		HCV	Lingual Gyrus	0.0215	0.0249
			Cuneus Cortex	0.0206	0.0623
			Lateral Occipital Cortex	0.0188	0.0273